Hindawi
Advances in Materials Science and Engineering
Volume 2019, Article ID 6812092, 11 pages
https://doi.org/10.1155/2019/6812092

Research Article

Elements-Added Diamond-Like Carbon Film for Biomedical Applications

Narin Sunthornpan,[1] **Shuichi Watanabe**,[2] **and Nutthanun Moolsradoo**[1]

[1]*King Mongkut's University of Technology Thonburi, Bangkok 10140, Thailand*
[2]*Nippon Institute of Technology, Saitama 345-8501, Japan*

Correspondence should be addressed to Nutthanun Moolsradoo; nutthanun.moo@kmutt.ac.th

Received 5 November 2018; Revised 17 January 2019; Accepted 4 February 2019; Published 3 March 2019

Academic Editor: Fernando Lusquiños

Elements-added diamond-like carbon films for biomedical applications were investigated. The aim of this work was to study the effects of the elemental contents (silicon and silicon-nitrogen) in a DLC film on its properties for biomedical applications. Pure DLC, Si-DLC, and Si-N-DLC films were prepared from C_2H_2, C_2H_2 : TMS, and C_2H_2 : TMS : N_2 gaseous mixtures, deposited on an AISI 316L substrate using the plasma-based ion implantation (PBII) technique. The structure of films was analyzed using Raman spectroscopy. The chemical composition of films was measured using energy dispersive X-ray spectroscopy (EDS). The average surface roughness of films was measured by using a surface roughness tester. The hardness and elastic modulus of films were measured by using a nanoindentation hardness tester. The friction coefficient of films was determined using a ball-on-disk tribometer. The surface contact angle was measured by a contact angle measurement. The corrosion performance of each specimen was measured using potentiodynamic polarization. The biocompatibility property of films was conducted using the MTT assay cytotoxicity test. The results indicate that the Si-N-DLC film shows the best hardness and friction coefficient (34.05 GPa and 0.13, respectively) with a nitrogen content of 0.5 at.%N, while the Si-DLC film with silicon content of 14.2 at.%Si reports the best contact angle and corrosion potential (92.47 and 0.398 V, respectively). The Si-N-DLC film shows the highest cell viability percentage of 81.96%, which is lower than the uncoated AISI 316L; this is a considerable improvement. All specimens do not demonstrate any cytotoxicity with approximate viabilities between 74% and 107%, indicating good biocompatibilities.

1. Introduction

Implantable biomedical devices are one of the most popular methods of medical field to treat human illnesses. There are many kinds of biomedical devices, such as vascular stents, artificial joints, artificial knees, and bone plates [1]. Most biomedical devices are made from stainless steel and titanium alloys because of the favorable mechanical and biocompatibility properties of these materials [2–5].

However, problems arising from material deterioration are often detected after long-term use. Corrosion is unavoidable due to various ions in the body reacting electrochemically with the surface of these metallic materials [6]. A metal device may release metal into the body, causing allergic reactions as thrombogenicity of the blood in complicated and aggressive physiological environments. Thus, ideal biomedical devices provide biocompatibility that prevents metallic ion release [6]. Surface coatings can improve both the mechanical properties and biocompatibility of biomedical devices that are in direct contact with blood and tissue.

Coating film technology has been studied for biomedical applications and includes diamond-like carbon (DLC) film. DLC films have many excellent properties including high hardness, low friction coefficient, good corrosion resistance, and good biocompatibility properties [7–10]. Additionally, DLC films can be doped with certain elements, such as hydrogen (H-DLC), fluorine (F-DLC), and sulfur (S-DLC), to improve performance. Previous studies have shown that DLC films doped with silicon (Si-DLC) are significantly improved corrosion properties due to the formation of a passive film on their surfaces [11–16]. Moreover, silicon-doped DLC films deposited by the sputtering method with the Si concentration varied from 4 to 16 at.% can reduce platelet adhesion on the material surface by modifying the

hydrophobicity of the material [17]. Additionally, the corrosion resistance of a pure DLC film can be increased via silicon and nitrogen doping by increasing the number of sp^3 sites in the film [18].

Plasma-based ion implantation (PBII) has been developed to improve DLC film properties and fabricate three-dimensional (3D) materials with complex shapes. In this technique, low working temperature avoids film quality degradation, such as loose and rough surface structure, and avoids DLC graphitization caused by normal CVD technique which is performed at higher working temperature [19, 20].

Currently, there is no report on the deposition of Si- and Si-N-added DLC films on the AISI 316L substrates by the PBII method aimed at comparing the mechanical, tribological, and corrosion performance, especially to compare the cell viability percentage.

In this paper, plasma-based ion implantation (PBII) was utilized to prepare different elements including silicon- and silicon-nitrogen-added DLC films (henceforth denoted as Si-DLC and Si-N-DLC films). The aim of the study was to compare and study the effects of element contents on the deposition and properties of the films for biomedical applications.

2. Materials and Methods

A schematic of the PBII apparatus used in this study is shown in Figure 1 [18]. The inner dimensions of the vacuum chamber are $600 \times 630 \times 200\,mm^3$, and the chamber produced a residual pressure of approximately 1×10^{-4} Pa. Plasma was generated from a radio frequency (RF, 13.6 MHz) glow discharge and a negative high-voltage pulse power supply connected to the sample holder.

Medical-grade AISI-type 316L stainless steel was used for the substrate material. Prior to plasma coating, specimens were polished down to 2000 grits using standard abrasive paper and the mirror was polished with 1 μm diamond paste and then cleaned in an ultrasonic cleaning bath. Substrates were sputter-cleaned with Ar^+ for 20 min to remove surface contaminants and surface oxides using a −10 kV pulse bias voltage. The DLC film interlayer was then deposited with CH_4 for 60 min to improve adhesion between the film and the substrate using a bias voltage of −20 kV. The RF power was set at 300 W, and the pressures of the sputter-cleaning and interlayer deposition were both 1 Pa. A pulse width of 5 μs, a pulse delay of 25 μs, and a pulse frequency of 1 kHz were used during the sputter-cleaning and interlayer deposition processes. Pure DLC, Si-DLC, and Si-N-DLC films were deposited using the PBII technique. The pure DLC film was used with a C_2H_2 precursor gas. The Si-DLC film was prepared from gaseous mixtures of C_2H_2 and TMS at three different flow rate ratios (1 : 2, 1 : 4, and 1 : 6). The Si-N-DLC film was deposited from gaseous mixtures of C_2H_2 : TMS : N_2 at three different flow rate ratios (14 : 1 : 2, 14 : 1 : 4, and 14 : 1 : 6). The bias voltage and deposition pressure of all of the films were set at −5 kV and between 2 and 2.5 Pa, respectively. The RF power was set at 300 W, and the pulse frequency was set to 1 kHz at a pulse width of 5 μs and a pulse delay of 25 μs. The thickness of each film was approximately 500 nm. The deposition conditions for the DLC, Si-DLC, and Si-N-DLC films are shown in Table 1.

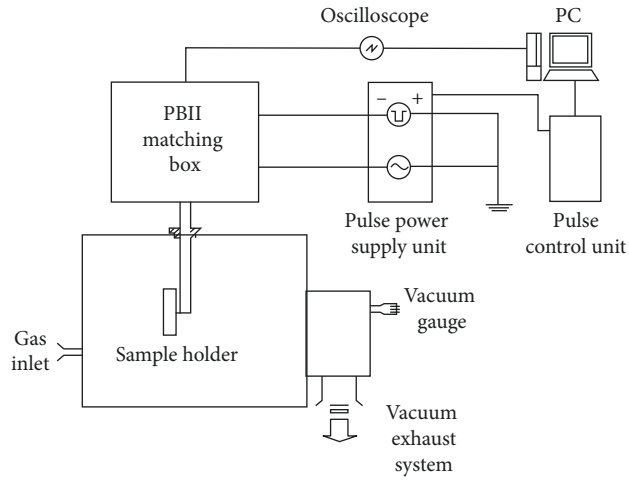

Figure 1: Schematic of the PBII apparatus used in this experiment [18].

The structures of the films were analyzed using Raman spectroscopy (JASCO NRS-1000 DT; beam diameter = 4 μm and wavelength = 532 nm). The chemical composition of films was measured using energy dispersive X-ray spectroscopy (EDS). The average surface roughness (R_a) at the top surface of the films was measured using a surface roughness tester (MAHR; MARSURF PS 10; length of travel = 4.8 mm, and cutoff length = 0.8 mm). The hardness and elastic modulus of films were measured using a nanoindentation hardness tester using a diamond ball indenter (Berkovich-type) with an indentation load of 1,000 μN. The friction coefficients of the films were determined using a ball-on-disk tribometer under ambient air conditions. In the friction test, a dry sliding test was performed using a ball indenter made of AISI 440C (SUS 440C, diameter of 6.0 mm) under a normal applied load of 1 N, a rotational radius of 4 mm, a linear speed of 31.4 mm/s, and 3,000 frictional rotations. The surface contact angle was measured by using a contact angle measurement device from Kyowa Interface Science Co., Ltd. using 1 μL of distilled water. The corrosion performance of each specimen was measured using potentiodynamic polarization in a simulated physiological Ringer's solution (ASTM F2129-17) at a pH of 7.5. A Pt sheet and Ag/AgCl were used as the counter and the reference electrodes, respectively. The potential voltage was varied from −1 V up to +1 V at a scanning rate of 1 mV/s. The cytotoxicity was selected for testing from the most abundant element added to the AISI 316L substrate; these were the pure DLC, Si-DLC 1 : 6, and Si-N-DLC 14 : 1 : 6 based on the ISO 10993-5 guidelines using the Dulbecco's modified Eagle medium (DMEM) dilution method. All samples were placed in sterile Duran bottles and then sterilized at 121°C for 15 min. L929 fibroblast cells (mouse fibroblasts) at 1×10^5 cells/mL were grown in a 96-well plate at a volume of 100 μL/well and then kept in an incubator (37°C, 5% CO_2) for 24 hours. The cell

Table 1: Deposition of pure DLC, Si-DLC, and Si-N-DLC films.

Film type	Gaseous mixture	Bias voltage (kV)	RF power (W)	Deposition pressure (Pa)	Gas flow rate ratio	Actual gas flow (sccm)
Pure DLC	C_2H_2	−5	300	2	—	17
Si-DLC	C_2H_2 : TMS	−5	300	2	1 : 2 1 : 4 1 : 6	5.5 : 11.0 3.2 : 12.8 2.5 : 15.0
Si-N-DLC	C_2H_2 : TMS : N_2	−5	300	2–2.5	14 : 1 : 2 14 : 1 : 4 14 : 1 : 6	14 : 1 : 2 14 : 1 : 4 14 : 1 : 6

viability was measured using an MTT assay and a microplate reader. This assay was performed in triplicate on cells seeded onto a 96-well plate.

3. Results and Discussion

3.1. Structure of Films by Raman Spectroscopy. Raman spectroscopy was used to investigate the DLC film's structure due to its nondestructive mechanism. The Raman spectra measured are shown in Figures 2–4 and indicate that the Raman spectra of pure DLC, Si-DLC, and Si-N-DLC films deposited at different flow rate ratios onto the fabricated AISI 316L substrates. The Raman spectra in the wavelength of 1,000 cm^{-1}–1,800 cm^{-1} were deconvoluted into Gaussian D and G peaks. The Raman spectrum was measured by curve fitting procedure using two Gaussian distribution peak shapes as show in Figure 2. The peak position and I_D/I_G ratio of the integrated areas by the D and G band in the DLC films fabricated with various gaseous mixtures and gaseous ratios are presented in Table 2. It has been obtained that the position of G band is related to the bond-angle disorder or sp^3 bonding content, while the I_D/I_G ratio is related to disorder [16, 21]. The films in this experiment show a broad spectrum composed of a D band (1,350 cm^{-1}) and a G band (1,580 cm^{-1}), which are similar to the peaks produced by conventional DLC films.

The results shown in Figures 3 and 4 and Table 2 show that the G peak and I_D/I_G ratio of pure DLC decrease due to silicon and silicon-nitrogen incorporation. For the Si-DLC film, the G peak tends to decrease from 1467 cm^{-1} (C : Si/1 : 2) to 1456 cm^{-1} (C : Si/1 : 6), while the I_D/I_G ratio decreases from 0.15 to 0.11 as the silicon content increases. This result is likely due to the altered microstructure as more sp^3 structures form as the silicon content increases. Additionally, longer destrained bonds vibrate at a lower frequency, leading to the G band shifting to a lower frequency. This outcome can be partially attributed to a reduction in compressive stress when silicon is introduced into the films [12].

For the Si-N-DLC film, the G peak tends to increase slightly from 1521 cm^{-1} (C : Si : N = 14 : 1: 2) to 1524 cm^{-1} (C : Si : N = 14 : 1 : 6), while the I_D/I_G ratio increases from 0.55 to 0.58 due to silicon-nitrogen incorporation. These results were likely caused by unstable sp^3 cluster formation and the increasing number or size of the film's graphitic structure due to nitrogen incorporation. These results thus suggest that the formation of a higher sp^2 and lower sp^3 clusters in the film is caused by an increase in the silicon-nitrogen content [22].

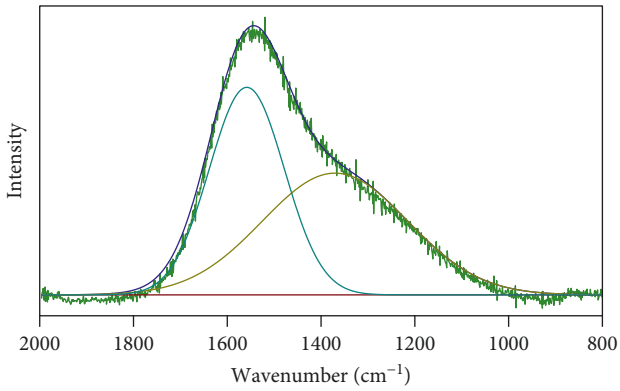

Figure 2: Raman curves fitting of DLC film.

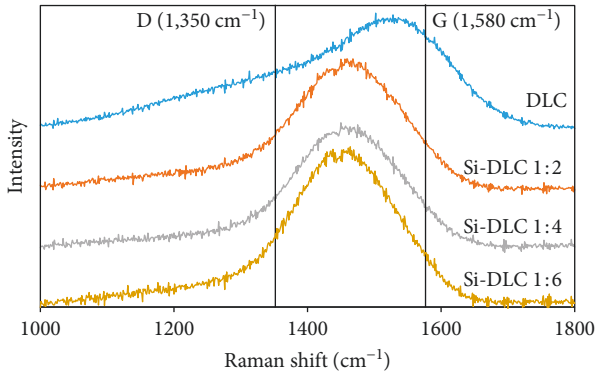

Figure 3: Raman spectra of pure DLC and Si-DLC films at different flow rate ratios.

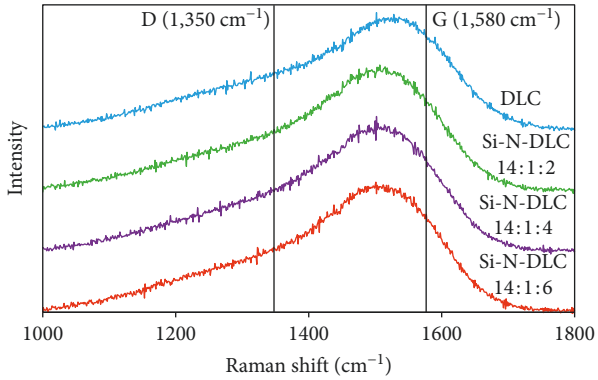

Figure 4: Raman spectra of pure DLC and Si-N-DLC films at different flow rate ratios.

Table 2: G peak and ID/IG ratio of pure DLC, Si-DLC, and Si-N-DLC films.

Film type	Gaseous mixture	Gas flow rate ratio	G peak (cm^{-1})	I_D/I_G
Pure DLC	C_2H_2	—	1,540	0.59
Si-DLC	C_2H_2 : TMS	1 : 2	1,467	0.15
		1 : 4	1,462	0.12
		1 : 6	1,456	0.11
Si-N-DLC	C_2H_2 : TMS : N_2	14 : 1 : 2	1,521	0.55
		14 : 1 : 4	1,520	0.56
		14 : 1 : 6	1,524	0.58

3.2. Relative Atomic Content of Films. The relative atomic contents measured on the top surface of the films deposited on the stainless-steel substrate are shown in Table 3. The carbon (C), silicon (Si), nitrogen (N), oxygen (O), and iron (Fe) concentrations were measured using the EDS, and values are shown in units of atomic percent (at.%). Concentrations were normalized to a total of 100 at.% and ignored the contribution of hydrogen because the hydrogen content could not be measured by EDS. The results also show that Fe appeared in all films, likely due to the thin film thickness (approximately 500 nm). It is assumed that the penetration depth of the electrons during the test is higher than the film thickness [18].

As shown in Table 3, the DLC film exhibits the highest C content (91.1 at.%), while the Si-DLC film shows that the Si content increased from 13.3 to 14.2 at.% by changing the gas flow rate from 1 : 2 to 1 : 6. The concentration of the Si-N-DLC film shows that the N content increased from 0.2 to 1.0 at.% when the gas flow rate changed from 14 : 1:2 to 14 : 1:6. In addition, a part of the EDS broad spectrum of Si-N-DLC film at the ratio of 14 : 1:6 is shown in Figure 5.

3.3. Surface Hardness and Elastic Modulus of Films. The hardness and elastic modulus of a film are important for biomedical application because contact pressures in some applications, such as artificial knees and joint replacements, may cause excessive material wear. The wear resistance of a material is directly related to its hardness and elastic modulus.

Each film's hardness and elastic modulus were determined on its top surface using a nanoindentation hardness test and a diamond ball indenter (Berkovich-type) with an indentation load of 1,000 μN. The hardness and elastic modulus of pure DLC, Si-DLC, and Si-N-DLC are shown in Figures 6 and 7 and Table 4.

As shown in Table 4, the hardness and elastic modulus of the films increased from those of pure DLC (25.46 GPa and 184.51 GPa, respectively) as the silicon content increased. For Si-DLC, the hardness and elastic modulus increased from 29.16 GPa (13.3 at.%Si) to 31.15 GPa (13.7 at.%Si) and 209.76 GPa to 216.92 GPa when the TMS flow rate ratio increased. The increased hardness and elastic modulus due to the change in microstructure was observed via the Raman analysis; the formation of sp^3 site structures increased the hardness and elastic modulus as the silicon content increased [18, 23]. However, the hardness and elastic modulus of the 1 : 6 Si-DLC film (14.2 at.%Si) decreased to 26.05 and 185.85 GPa, respectively. C_2H_2 and TMS used during fabrication: when the TMS flow rate increased, the hydrogen content in the film increased. The polymeric sp^3 C–H bonds established due to the high hydrogen concentration decreased the film's hardness [23]. Si-DLC films are likely to be saturated with hydrogen, especially when using a TMS precursor. The same trend verifies the reliability of our results.

The Si-N-DLC film exhibited the high hardness and elastic modulus values 34.05 GPa and 220.97 GPa (0.5 at.%N), respectively, despite its number and size of sp^3 clusters being lower than those of the Si-DLC film. The formation of C–N bonds yielded high hardness and elastic modulus values because C–Si bonds are weaker than C–N bonds. However, when the nitrogen was increased to 1.0 at.%N, the hardness and elastic modulus decreased to 26.28 GPa and 185.61 GPa, respectively, which was likely due to the lower bond strength of the N–Si network [24, 25].

3.4. Friction Coefficient of Films. The friction coefficients of pure DLC, Si-DLC, and Si-N-DLC films were determined under ambient air conditions and are shown in Figure 8. The effects of the silicon and silicon-nitrogen contents on the friction coefficients of the Si-DLC and Si-N-DLC films were investigated. The results indicate that all coating films can increase the low friction coefficient of AISI 316L.

The friction coefficient of pure DLC was 0.17. It was found that increasing the silicon content in the film increased the film's friction coefficient. The Si-DLC film's friction coefficient increased from 0.22 (13.3 at.%Si) to 0.30 (14.2 at.%Si) when the TMS flow rate ratio increased, which reduced the carbon content in the film. In general, carbon acts as a solid lubricant that reduces friction between ball-film contact areas [26, 27]. Additionally, for the Si-DLC film, the friction coefficient also increased due to the film's lower surface hardness and elastic modulus. The contact area at the ball-film interface actually increased as the film hardness and elastic modulus decreased, resulting in the film surface having difficulty supporting the high load induced by the friction coefficient [28]. The Si-N-DLC film exhibited the lowest friction coefficient (0.13 at 0.5 at.%N) due to the film's high hardness and elastic modulus. The film's low friction coefficient can be attributed to the lubricating effect of the sp^2 cluster in the film coatings, as shown in Table 2 [29].

3.5. Contact Angle of Films. The contact angles measured on the top surfaces of the films are shown in Table 5. A volume of 1 μL of distilled water was released onto the top surface of the films under atmospheric conditions at room temperature.

Many studies have shown that surface roughness and surface hydrophilicity strongly increase the blood compatibility of implants: a smooth and hydrophobic surface is beneficial to the blood compatibility [21, 30, 31].

Table 3: Relative atomic content and average roughness of pure DLC, Si-DLC, and Si-N-DLC films.

Film type	Gaseous mixture	Gas flow rate ratio	Relative atomic content (at.%)					Average roughness (R_a; μm)
			C	Si	N	O	Fe	
Uncoated AISI 316 L	—	—	5.9	0.8	—	3.6	61.7	0.18
Pure DLC	C_2H_2	—	91.1	0.1	—	0.3	5.8	0.13
Si-DLC	C_2H_2 : TMS	1 : 2	62.7	13.3	—	2.7	14.4	0.08
		1 : 4	59.1	13.7	—	3.1	17.1	0.07
		1 : 6	58.1	14.2	—	2.8	16.9	0.08
Si-N-DLC	C_2H_2 : TMS : N_2	14 : 1 : 2	86.3	2.8	0.2	0.7	6.9	0.08
		14 : 1 : 4	77.9	1.7	0.5	1.9	12.3	0.07
		14 : 1 : 6	81.6	1.9	1.0	1.2	9.8	0.10

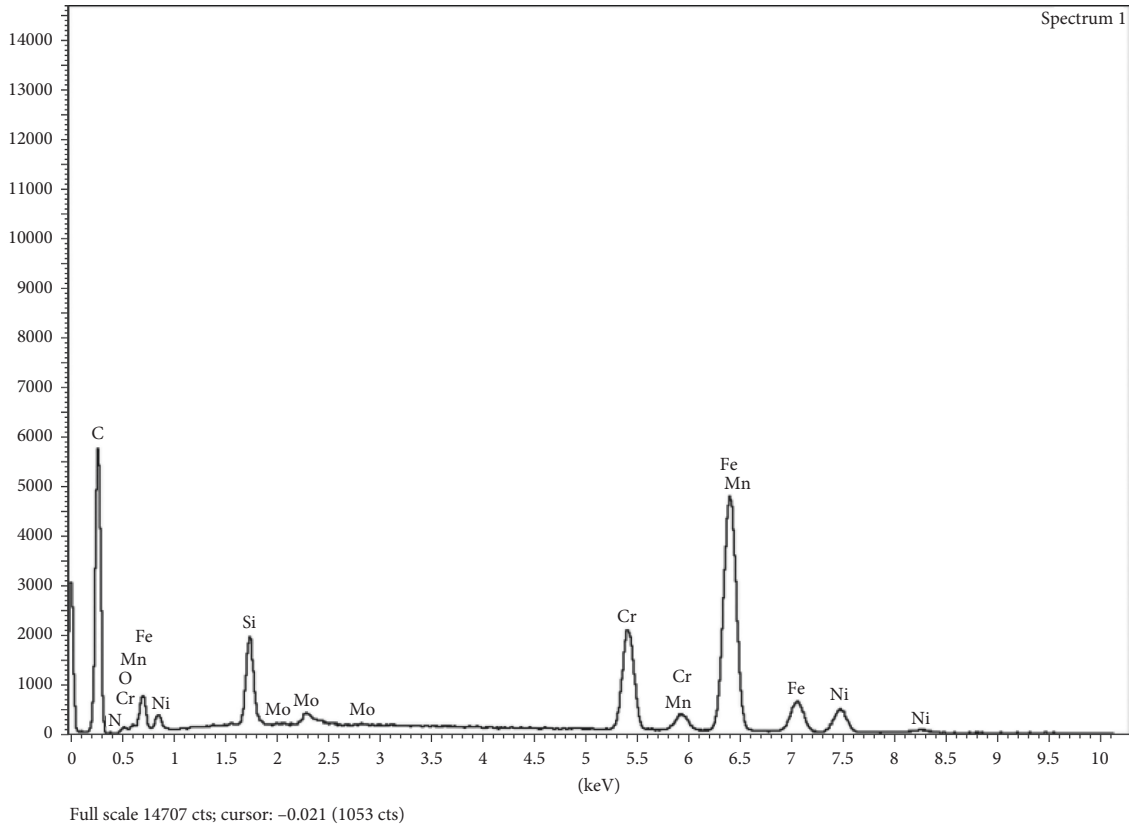

Figure 5: EDS broad spectrum of Si-N-DLC film at a ratio of 14 : 1 : 6.

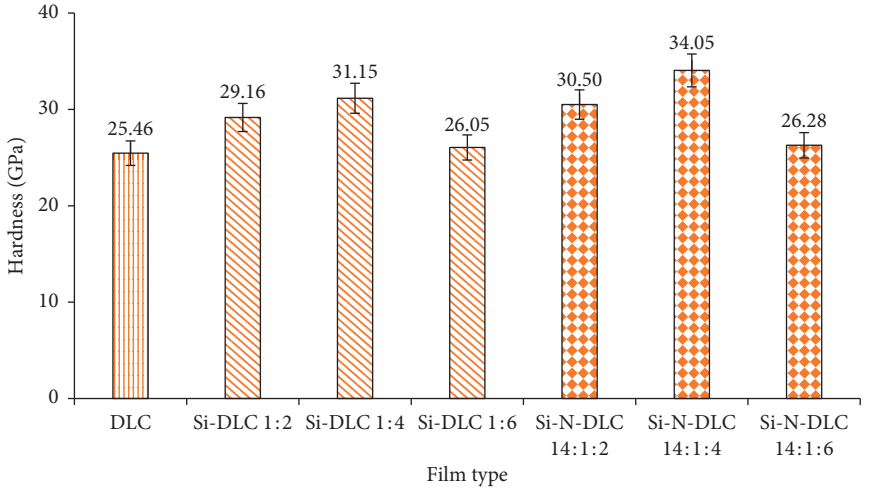

Figure 6: Hardness of pure DLC, Si-DLC, and Si-N-DLC films.

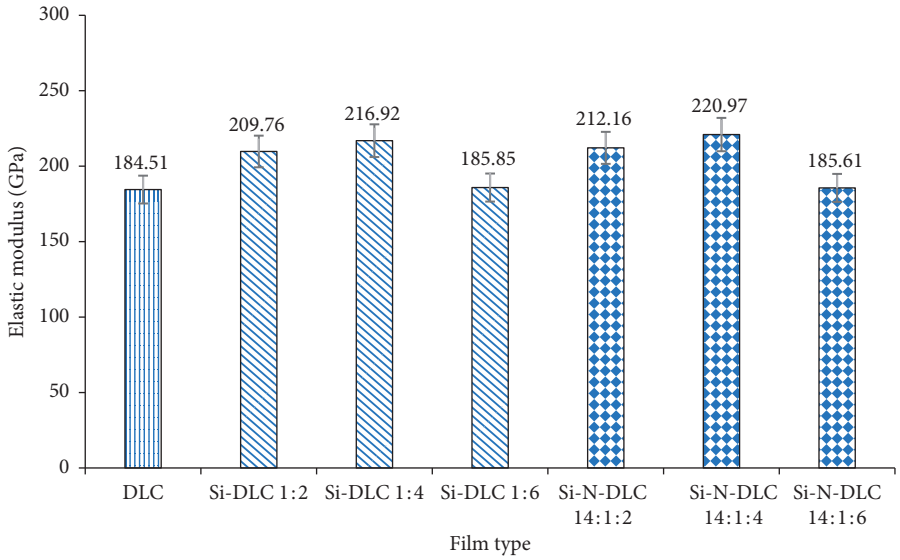

Figure 7: Elastic modulus of pure DLC, Si-DLC, and Si-N-DLC films.

Table 4: Mechanical properties and friction coefficient of pure DLC, Si-DLC, and Si-N-DLC films.

Film type	Gas flow rate ratio	Mechanical properties		Friction coefficient
		Hardness (GPa)	Elastic modulus (GPa)	
Uncoated AISI316L	—	—	—	1.09
Pure DLC	—	25.46	184.51	0.17
Si-DLC	1 : 2	29.16	209.76	0.22
	1 : 4	31.15	216.92	0.21
	1 : 6	26.05	185.85	0.30
Si-N-DLC	14 : 1 : 2	30.50	212.16	0.17
	14 : 1 : 4	34.05	220.97	0.13
	14 : 1 : 6	26.28	185.61	0.15

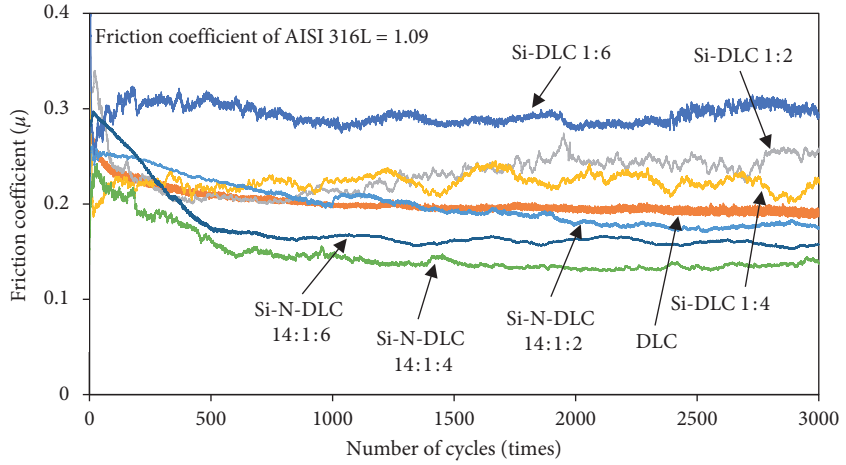

Figure 8: Friction coefficient of pure DLC, Si-DLC, and Si-N-DLC films.

Contact-angle studies play an important role in understanding the surface phenomena of the substrates.

The polished smooth surface of AISI 316L reported a contact angle value of 93.47°, describing the hydrophobic nature of AISI 316L [32, 33]. The contact angle value reduced to 79.33° for the pure DLC film. For the Si-DLC film, the contact angle increased from 88.93° (13.3 at.%Si) to 92.47° (14.2 at.%Si) as silicon content increased. This was likely due to the decreasing surface energy of the films as the silicon content increased and more strongly influenced the

Table 5: Surface contact angle, corrosion potential (E_{corr}), and corrosion current density (i_{corr}) of pure DLC, Si-DLC, and Si-N-DLC films.

Film type	Gas flow rate ratio	Contact angle (°)	Corrosion potential (E_{corr} (V))	Corrosion current density (i_{corr} (A/cm^2))
Uncoated AISI316L	—	93.47	−0.125	$2.49E-6$
Pure DLC	—	79.33	−0.010	$0.949E-6$
Si-DLC	1 : 2	88.93	0.198	$0.887E-6$
	1 : 4	92.20	0.199	$0.909E-6$
	1 : 6	92.47	0.398	$0.280E-6$
Si-N-DLC	14 : 1 : 2	77.87	−0.001	$0.931E-6$
	14 : 1 : 4	76.23	0.004	$0.648E-6$
	14 : 1 : 6	77.53	0.198	$0.570E-6$

hydrophobic property of the film [34]. Moreover, the contact angle was relatively unaffected by surface roughness, as shown in Table 3.

For the Si-N-DLC film, the contact angle was found to be related to the nitrogen and carbon atomic concentration ratio. The contact angle decreased as the nitrogen content increased, as shown in Table 5. The contact angle of the Si-N-DLC film shifted slightly as the gas flow rate changed from 14 : 1 : 2 to 14 : 1 : 6. The Si-N-DLC surface was thus more hydrophilic than the pure DLC and Si-DLC films, which might be due to an increase in the dispersive and polarity components of surface energy from the high number of nucleophilic electrons produced by the formation of N–H and C=N networks [35].

3.6. Corrosion Resistance Property of Films. Biocompatibility is simply defined as the performance of a material to be permitted by the body. A foreign body is created when materials are implanted in a body and is directly related to the corrosion behavior of the material due to the tendency for the alloy to release potential toxic ions from corrosion behavior [36].

In general, samples with greater corrosion potential and lower current density provide better corrosion performance. An improvement in the corrosion resistance of a film is demonstrated by a shift in the polarization curve towards a region of lower current density and greater potential [37]. Additionally, variation in the film microstructure allows different corrosion behaviors to occur [38]. Generally, a more prevalent sp^3 structure tends to increase electrochemical corrosion resistance [18, 38].

Figures 9 and 10 show the potentiodynamic curves for uncoated AISI 316 L, pure DLC, Si-DLC, and Si-N-DLC films. Table 5 summarizes the electrochemical parameters measured from the potentiodynamic polarization curves shown in Figures 9 and 10. All films show higher corrosion potential (E_{corr}) and lower current density (i_{corr}) than the uncoated AISI 316 L sample. Pure DLC shows a corrosion potential and current density of −0.010 V and 0.949×10^{-6} A, respectively. Corrosion potential increased, and current density decreased due to silicon (Si-DLC) and silicon-nitrogen (Si-N-DLC) incorporation. For the Si-DLC film, corrosion potential (E_{corr}) increased from 0.198 V to 0.398 V and current density (i_{corr}) decreased from 0.887×10^{-6} A/cm^2 to 0.280×10^{-6} A/cm^2 due to silicon incorporation. For the Si-N-DLC film, corrosion potential (E_{corr}) increased from −0.001 V to 0.198 V and current density (i_{corr}) decreased from 0.931×10^{-6} A/cm^2 to 0.570×10^{-6} A/cm^2 due to silicon-nitrogen incorporation. Thus, the best corrosion resistance was observed in the Si-DLC film with a silicon content of 14.2 at.%Si with corrosion potential (E_{corr}) and current density (i_{corr}) values of 0.398 V and 0.280×10^{-6} A/cm^2, respectively. The greater corrosion resistance of the Si-DLC and Si-N-DLC films than that of the uncoated AISI 316L and pure DLC film shows that the incorporation of silicon and silicon-nitrogen into the pure DLC film improves corrosion resistance. This outcome is likely due to the increased number of sp^3 sites in the film's structure [39] and the creation of a silicon oxide passive film on the film's surface [11]. Additionally, the sp^3 structure created via silicon incorporation can reduce the internal stress that causes the corrosion [12]. Additionally, the results show more corrosion-resistant potential than the previous report mentioned above [14]. The report showed the corrosion potential and current density of Si-DLC up to 1.5×10^{-5} mA/cm^2 and −0.7 V with high silicon content of 30 at.% [14].

3.7. Cytotoxicity Test of Films. A cytotoxic test was designed according to ISO 10993-5 standard, and L 929 fibroblast cells were used in this method. The cytotoxic test is typically used to evaluate materials for biomedical applications to confirm their implantability. The cell viability percentage of uncoated AISI 316L, pure DLC, Si-DLC, and Si-N-DLC are shown in Figure 11.

Figures 11 and 12 show the viability and morphology of the L929 fibroblast cells after being exposed to the MTT solution. The Si-N-DLC film exhibited a cell viability of 81.96%, which is lower than the uncoated AISI 316 L (107%) but higher than the pure DLC (78.16%) and the Si-DLC films (74.4%). However, none of the specimens were found to be cytotoxic. Cell viability ranged from 74.4% to 107%, indicating good biocompatibility because viability percentages (live/dead %) were not lower than 50% as per ISO10993-5. Additionally, no visible change in cell morphology was observed; the cells still exhibited a typical fibroblastic morphology, as shown in Figure 12 [40]. These results agree with those reported by Sui et al. [21], Gotzmann et al. [41], Bociaga et al. [42], and Antunes et al. [43].

4. Conclusions

Elements-added diamond-like carbon films were investigated for biomedical applications. Pure DLC, Si-DLC, and Si-N-DLC films were prepared on an AISI 316L

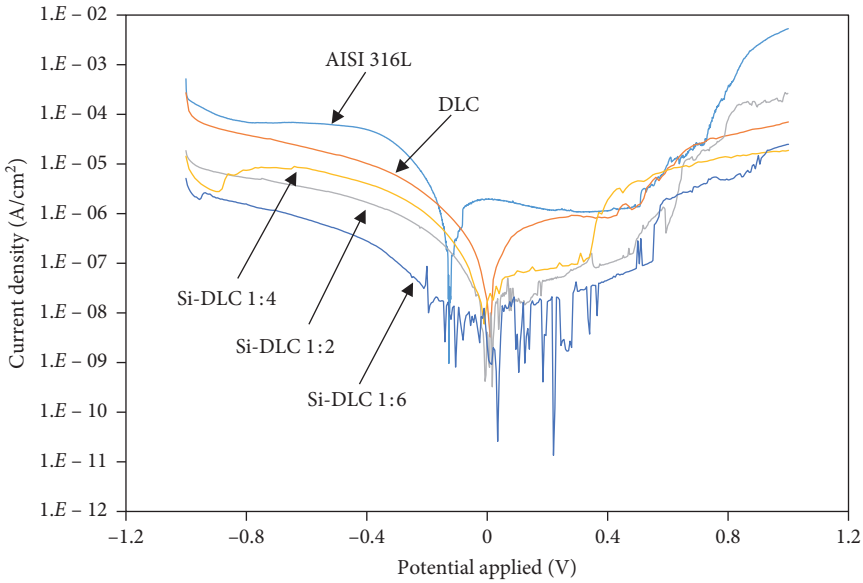

Figure 9: Potentiodynamic polarization curve of uncoated AISI 316 L pure DLC and Si-DLC films.

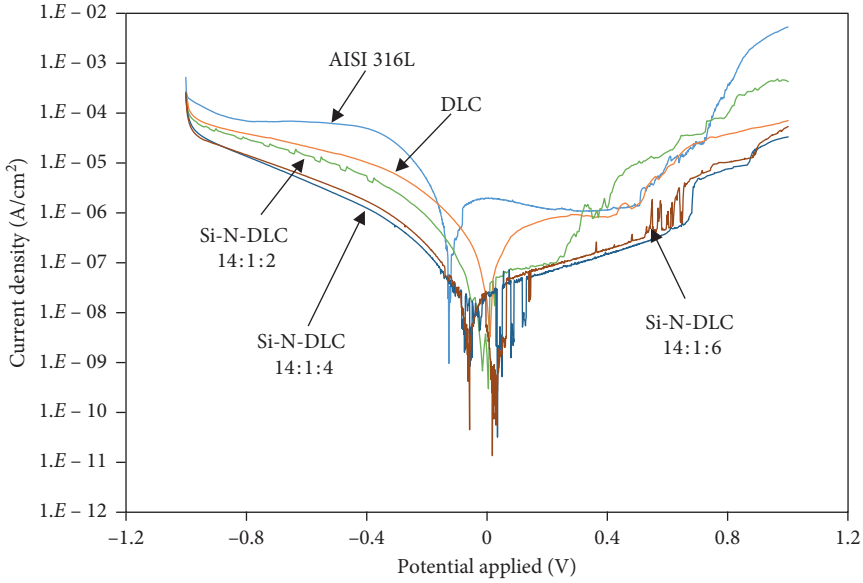

Figure 10: Potentiodynamic polarization curve of uncoated AISI 316 L pure DLC and Si-N-DLC films.

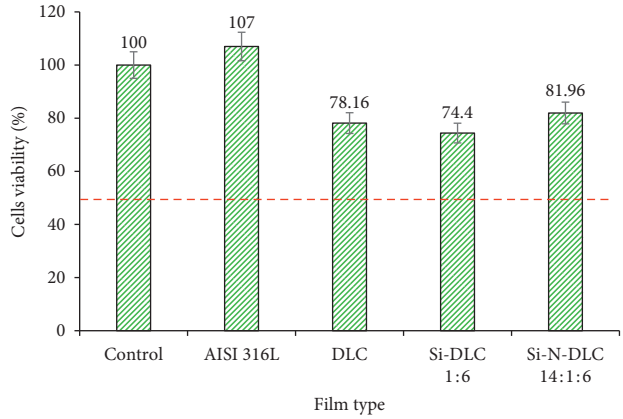

Figure 11: The cells viability of all films by using the DMEM elution method.

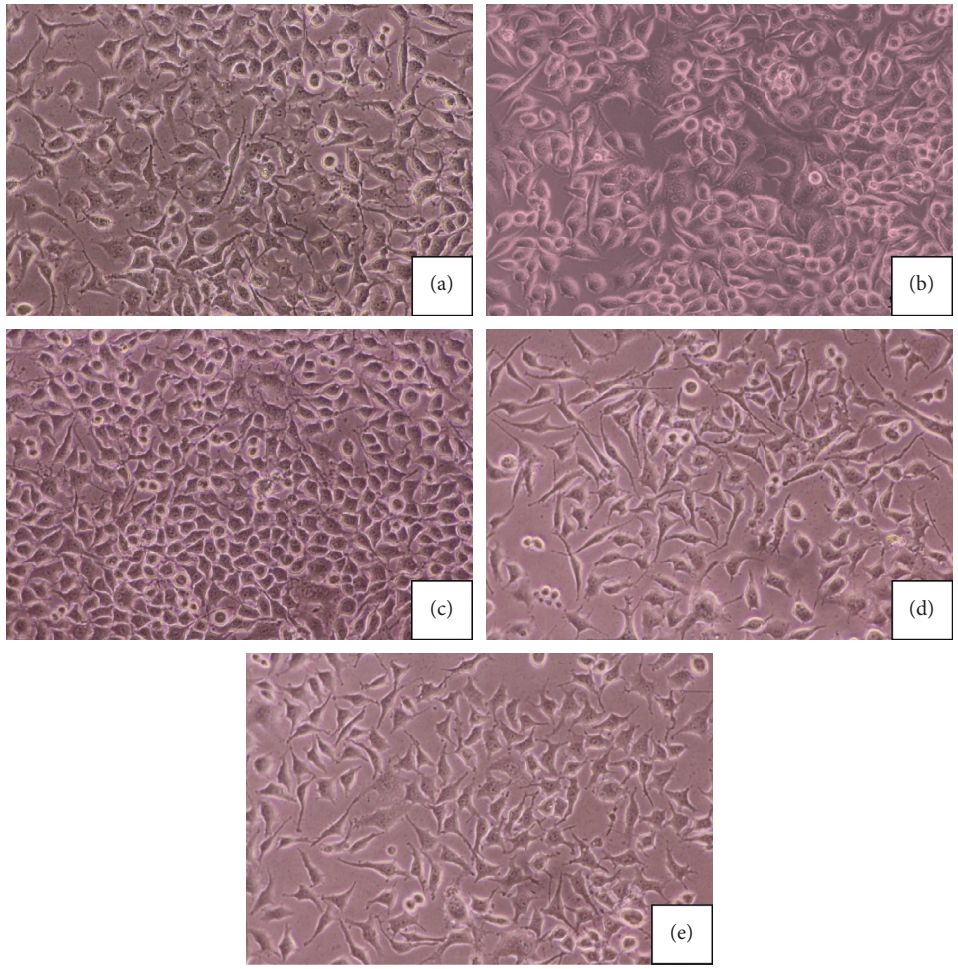

Figure 12: Indirect contact assay of AISI 316L was coated following the ISO 10993-5 standard for the MTT cytotoxicity test by using the L929 cells: (a) control, (b) AISI 316 L (c) pure DLC, (d) Si-DLC 1 : 6, and (e) Si-N-DLC 14 : 1 : 6.

substrate at different flow rate ratios and gaseous mixtures using the plasma-based ion implantation (PBII) technique. All films were described in terms of structure, relative atomic content, surface roughness, hardness, elastic modulus, friction coefficient, contact angle, corrosion resistance, and cytotoxicity. Hardness, elastic modulus, friction coefficient, contact angle, and corrosion resistance increased as the silicon content in the Si-DLC film decreased. Increasing the silicon-nitrogen content in the Si-N-DLC film also increased the hardness and corrosion resistance of the film but decreased the friction coefficient and contact angle. Changes in film hardness, friction coefficient, and corrosion resistance were related to changes in sp^3 site structures. Chemical bond strength also affected the hardness and elastic modulus of the films. The Si-N-DLC film showed the best hardness and friction coefficient (34.05 GPa and 0.13, respectively) with a nitrogen content of 0.5 at.%N, while the Si-DLC film with silicon content of 14.2 at.%Si reported the best contact angle and corrosion potential (92.47° and 0.398 V, respectively). The Si-N-DLC film showed the highest cell viability percentage of 81.96%, which was lower than the uncoated AISI 316L; this is a considerable improvement. The DLC and Si-DLC films showed cell viability percentages of 78.16% and 74.4%, respectively. All specimens did not demonstrate any cytotoxicity with approximate viabilities between 74% and 107%, indicating good biocompatibilities.

Data Availability

No data were used to support this study.

Disclosure

A part of this manuscript abstract has been presented in ICASS 2017-Oxford Abstracts.

Conflicts of Interest

The authors declare that they have no conflicts of interest.

Acknowledgments

This study was supported by a Petchra Pra Jom Klao Master's Degree Research Scholarship from King Mongkut's University of Technology Thonburi.

References

[1] V. Braic, M. Braic, M. Balaceanu et al., "(Zr,Ti)CN coatings as potential candidates for biomedical applications," *Surface and Coatings Technology*, vol. 206, no. 4, pp. 604–609, 2011.

[2] X. Liu, P. Chu, and C. Ding, "Surface modification of titanium, titanium alloys, and related materials for biomedical applications," *Materials Science and Engineering: R: Reports*, vol. 47, no. 3–4, pp. 49–121, 2004.

[3] H. Zhou, M. Jiang, Y. Xin et al., "Surface deposition of graphene layer for bioactivity improvement of biomedical 316 stainless steel," *Materials Letters*, vol. 192, pp. 123–127, 2017.

[4] H.-A. Pan, J.-Y. Liang, Y.-C. Hung, C.-H. Lee, J.-C. Chiou, and G. S. Huang, "The spatial and temporal control of cell migration by nanoporous surfaces through the regulation of ERK and integrins in fibroblasts," *Biomaterials*, vol. 34, no. 4, pp. 841–853, 2013.

[5] A. Amanov, S. W. Lee, and Y. S. Pyun, "Low friction and high strength of 316L stainless steel tubing for biomedical applications," *Materials Science and Engineering: C*, vol. 71, pp. 176–185, 2017.

[6] D. R. Mcclean and N. L. Eigler, "Stent design: implications for restenosis," *Reviews in Cardiovascular Medicine*, vol. 3, pp. 16–22, 2002.

[7] S. C. H. Kwok, J. Wang, and P. K. Chu, "Surface energy, wettability, and blood compatibility phosphorus doped diamond-like carbon films," *Diamond and Related Materials*, vol. 14, no. 1, pp. 78–85, 2005.

[8] R. Cruz, J. Rao, T. Rose, K. Lawson, and J. R. Nicholls, "DLC-ceramic multilayers for automotive applications," *Diamond and Related Materials*, vol. 15, no. 11-12, pp. 2055–2060, 2006.

[9] A. Shirakura, M. Nakaya, Y. Koga, H. Kodama, T. Hasebe, and T. Suzuki, "Diamond-like carbon films for PET bottles and medical applications," *Thin Solid Films*, vol. 494, no. 1-2, pp. 84–91, 2006.

[10] N. Moolsradoo, S. Abe, and S. Watanabe, "Thermal stability and tribological performance of DLC–Si–O films," *Advances in Materials Science and Engineering*, vol. 2011, Article ID 483437, 7 pages, 2011.

[11] M. Azzi, P. Amirault, M. Paquette, J. E. Klemberg-Sapieha, and L. Martinu, "Corrosion performance and mechanical stability of 316L/DLC coating system: role of interlayers," *Surface and Coatings Technology*, vol. 204, no. 24, pp. 3986–3994, 2010.

[12] P. Papakonstantinou, J. F. Zhao, P. Lemoine, E. T. McAdams, and J. A. McLaughlin, "The effects of Si incorporation on the electrochemical and nanomechanical properties of DLC thin films," *Diamond and Related Materials*, vol. 11, no. 3–6, pp. 1074–1080, 2002.

[13] N. Moolsradoo and S. Watanabe, "Deposition and tribological properties of sulfur-doped DLC films deposited by PBII method," *Advances in Materials Science and Engineering*, vol. 2010, Article ID 958581, 7 pages, 2010.

[14] J. Choi, S. Nakao, J. Kim, M. Ikeyama, and T. Kato, "Corrosion protection of DLC coatings on magnesium alloy," *Diamond and Related Materials*, vol. 16, no. 4–7, pp. 1361–1364, 2007.

[15] J. Choi, J. Kim, S. Nakao, M. Ikeyama, and T. Kato, "Friction properties of protective DLC films on magnesium alloy in aqueous NaCl solution," *Nuclear Instruments and Methods in Physics Research Section B: Beam Interactions with Materials and Atoms*, vol. 257, no. 1–2, pp. 718–721, 2007.

[16] J. Choi, S. Nakao, M. Ikeyama, and T. Kato, "Effect of deposition pressure on the properties of DLC coatings deposited by bipolar-type PBII&D," *Surface and Interface Analysis*, vol. 40, no. 3–4, pp. 806–809, 2008.

[17] D. Bociaga, M. Kaminska, A. Sobczyk-Guzenda, K. Jastrzebski, L. Swiatek, and A. Olejnik, "Surface properties and biological behaviour of Si-DLC coatings fabricated by a multi-target DC-RF magnetron sputtering method for medical applications," *Diamond and Related Materials*, vol. 67, pp. 41–50, 2016.

[18] N. Moolsradoo and S. Watanabe, "Influence of elements on the corrosion resistance of DLC films," *Advances in Materials Science and Engineering*, vol. 2017, Article ID 3571454, 6 pages, 2017.

[19] L. Xia, M. Sun, and J. Liao, "The effect of negative bias pulse on the bonding configurations and properties of DLC films prepared by PBII with acetylene," *Diamond and Related Materials*, vol. 14, no. 1, pp. 42–47, 2005.

[20] Y. Wang, X. Ma, G. Tang, and M. Sun, "Characterization of DLC films prepared by plasma-based ion implantation on AISI 321 steel," *Vacuum*, vol. 89, pp. 74–77, 2013.

[21] J. H. Sui, Z. Y. Gao, W. Cai, and Z. G. Zhang, "DLC films fabricated by plasma immersion ion implantation and deposition on the NiTi alloys for improving their corrosion resistance and biocompatibility," *Materials Science and Engineering: A*, vol. 454-455, pp. 472–476, 2007.

[22] S. C. Ray, W. F. Pong, and P. Papakonstantinou, "Iron, nitrogen and silicon doped diamond like carbon (DLC) thin films: a comparative study," *Thin Solid Films*, vol. 610, pp. 42–47, 2016.

[23] S. Fujimoto, N. Ohtake, and O. Takai, "Mechanical properties of silicon-doped diamond-like carbon films prepared by pulse-plasma chemical vapor deposition," *Surface and Coatings Technology*, vol. 206, no. 5, pp. 1011–1015, 2011.

[24] J. Wang, J. Ma, W. Huang, L. Wang, H. He, and C. Liu, "The investigation of the structures and tribological properties of F-DLC coatings deposited on Ti-6Al-4V alloys," *Surface and Coatings Technology*, vol. 316, pp. 22–29, 2017.

[25] D. R. Lide, *CRC Handbook of Chemistry and Physics, Internet Version 2005*, CRC Press, Boca Raton, FL, USA, 2005.

[26] C. S. Jang, J.-H. Jeon, P. K. Song, M. C. Kang, and K. H. Kim, "Synthesis and mechanical properties of TiAlCxN1−x coatings deposited by arc ion plating," *Surface and Coatings Technology*, vol. 200, no. 5-6, pp. 1501–1506, 2005.

[27] J. M. Lackner, W. Waldhauser, and R. Ebner, "Large-area high-rate pulsed laser deposition of smooth TiCxN1−x coatings at room temperature-mechanical and tribological properties," *Surface and Coatings Technology*, vol. 188-189, pp. 519–524, 2004.

[28] N. Moolsradoo and S. Watanabe, "Modification of tribological performance of DLC films by means of some elements addition," *Diamond and Related Materials*, vol. 19, no. 5-6, pp. 525–529, 2010.

[29] B. Saha, E. Liu, S. B. Tor, N. W. Khun, D. E. Hardt, and J. H. Chun, "Replication performance of Si-N-DLC-coated Si micro-molds in micro-hot-embossing," *Journal of Micromechanics and Microengineering*, vol. 20, no. 4, 8 pages, 2010.

[30] J. Wang and N. Jiang, "Blood compatibilities of carbon nitride film deposited on biomedical NiTi alloy," *Diamond and Related Materials*, vol. 18, no. 10, pp. 1321–1325, 2009.

[31] H. Yu, Y. Liu, Y. Wang et al., "A study on poly (N-vinyl-2-pyrrolidone) covalently bonded NiTi surface for inhibiting protein adsorption," *Progress in Natural Science: Materials International*, vol. 26, no. 6, pp. 584–589, 2016.

[32] A. M. Kumar, B. Suresh, S. Das, I. B. Obot, A. Y. Adesina, and S. Ramakrishna, "Promising bio-composites of polypyrrole

and chitosan: surface protective and in vitro biocompatibility performance on 316L SS implants," *Carbohydrate Polymers*, vol. 173, pp. 121–130, 2017.

[33] K. Pradeep PremKumar, N. Duraipandy, K. N. Syamala, and N. Rajendran, "Antibacterial effects, biocompatibility and electrochemical behavior of zinc incorporated niobium oxide coating on 316L SS for biomedical applications," *Applied Surface Science*, vol. 427, pp. 1166–1181, 2018.

[34] D. W. Ren, Q. Zhao, and A. Bendavid, "Anti-bacterial property of Si and F doped diamond-like carbon coatings," *Surface and Coatings Technology*, vol. 226, pp. 1–6, 2013.

[35] M. H. Ahmed and J. A. Byrne, "Effect of surface structure and wettability of DLC and N-DLC thin films on adsorption of glycine," *Applied Surface Science*, vol. 258, no. 12, pp. 5166–5174, 2012.

[36] T. Duerig, A. Pelton, and D. Stöckel, "An overview of nitinol medical applications," *Materials Science and Engineering: A*, vol. 273-275, pp. 149–160, 1999.

[37] J. H. Sui, Z. G. Zhang, and W. Cai, "Surface characteristics and electrochemical corrosion behavior of fluorinated diamond-like carbon (F-DLC) films on the NiTi alloys," *Nuclear Instruments and Methods in Physics Research Section B: Beam Interactions with Materials and Atoms*, vol. 267, no. 15, pp. 2475–2479, 2009.

[38] C. C. Wachesk, V. J. Trava-Airoldi, N. S. Da-Silva, A. O. Lobo, and F. R. Marciano, "The influence of titanium dioxide on diamond-like carbon biocompatibility for dental applications," *Journal of Nanomaterials*, vol. 2016, Article ID 8194516, 7 pages, 2016.

[39] N. W. Khun, E. Liu, and X. T. Zeng, "Corrosion behavior of nitrogen doped diamond-like carbon thin films in NaCl solutions," *Corrosion Science*, vol. 51, no. 9, pp. 2158–2164, 2009.

[40] R. W. Y. Poon, K. W. K. Yeung, X. Y. Liu et al., "Carbon plasma immersion ion implantation of nickel-titanium shape memory alloys," *Biomaterials*, vol. 26, no. 15, pp. 2265–2272, 2005.

[41] G. Gotzmann, J. Beckmann, C. Wetzel, B. Scholz, U. Herrmann, and J. Neunzehn, "Electron-beam modification of DLC coatings for biomedical applications," *Surface and Coatings Technology*, vol. 311, pp. 248–256, 2017.

[42] D. Bociaga, A. Sobczyk-Guzenda, W. Szymanski et al., "Mechanical properties, chemical analysis and evaluation of antimicrobial response of Si-DLC coatings fabricated on AISI 316 LVM substrate by a multi-target DC-RF magnetron sputtering method for potential biomedical applications," *Applied Surface Science*, vol. 417, pp. 23–33, 2017.

[43] R. A. Antunes, A. C. D. Rodas, N. B. Lima, O. Z. Higa, and I. Costa, "Study of the corrosion resistance and in vitro biocompatibility of PVD TiCN-coated AISI 316L austenitic stainless steel for orthopedic applications," *Surface and Coatings Technology*, vol. 205, no. 7, pp. 2074–2081, 2010.